IEEE Photonics Journal
An IEEE Photonics Society Publication

Open Access

The Optical Transmission Characteristic of Hollow Carbon-Coated Fe_3O_4 Colloidal Photonic Crystal

Volume 7, Number 1, February 2015

Yan Huang
Gongying Liang
Xuegang Lu
Xuejiao Bie
Wenyu Li

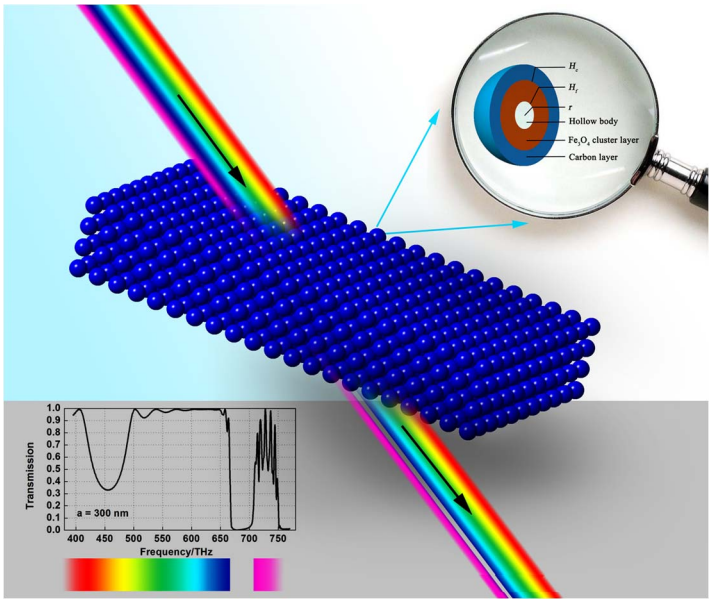

DOI: 10.1109/JPHOT.2014.2387258
1943-0655

IEEE photonics SOCIETY
IEEE

The Optical Transmission Characteristic of Hollow Carbon-Coated Fe_3O_4 Colloidal Photonic Crystal

Yan Huang, Gongying Liang, Xuegang Lu, Xuejiao Bie, and Wenyu Li

School of Science, Key Laboratory of Shaanxi for Advanced Materials and Mesoscopic Physics, State Key Laboratory for Mechanical Behavior of Materials, Xi'an Jiaotong University, Xi'an 710049, China

DOI: 10.1109/JPHOT.2014.2387258

Manuscript received October 24, 2014; revised December 6, 2014; accepted December 12, 2014. Date of publication January 1, 2015; date of current version January 27, 2015. This work was supported by the National Natural Science Foundation (No. 51172178) of P. R. China. Corresponding author: X. Lu (e-mail: xglu@mail.xjtu.edu.cn).

Abstract: The optical transmission characteristics for the hollow carbon-coated Fe_3O_4 colloidal photonic crystal have been calculated with the finite-difference time-domain (FDTD) method. We analyze the influence of the factors on the photonic band gap (PBG) that include lattice constant a, the number of the particles in propagating direction N_y, the thickness of carbon layer H_c and Fe_3O_4 cluster layer H_f, and the thickness ratio of the two layers. The results show that the PBGs red shift and the bandwidth first increases and then decreases with the increasing a. In the situation of increasing N_y, the PBG changes from irregular to uniform, followed by the oscillations on both sides of the PBG growing in number and the deepened PBG in the low-frequency region. The PBGs move toward the low frequency direction with the increase of H_c, and the optimal value of H_c for the uniform color response is 10 nm $\sim$ 25 nm. The PBGs red shift with the increasing H_f, and the first bandwidth increases while the second decreases. The optimal H_f for the ideal PBG is 35 nm $\sim$ 55 nm. The stop bands move to the high-frequency direction with the increasing thickness ratio $(H_c : H_f)$, and the best ratio is 10 nm : 55 nm for the complete PBG and wider bandwidth.

Index Terms: Photonic crystal, transmission characteristic, PBG, FDTD, carbon-coated Fe_3O_4, hollow structure.

1. Introduction

Yablonovitch [1] and John [2] independently suggested the concept of the "Photonic Crystal" in 1987. Researchers verified the existence of PBG in the diamond structure [3], based on the calculated results in 1990. Under the guidance of theoretical design, Yablonovitch fabricated the first complete PBG structure [4] with the band gap range of 10 GHz $\sim$ 13 GHz in 1991, and the results in theoretical calculation and experimental measurement matched well. This was the first time to experimentally verify the existence of PBG in materials. Generally speaking, when electromagnetic waves enter into the dielectric structure with the permittivity periodically arranged, due to the Bragg scattering, a certain frequency range of electromagnetic waves cannot propagate in this structure and finally form PBGs. The colloidal photonic crystals assembled by colloidal nanoparticles are a kind of very important PBG materials. Researchers

have gradually focussed on using the magnetic field to induce colloidal particles to form the photonic crystals in recent years. The superparamagnetic colloidal particle becomes the ideal building block of this kind of photonic crystal for its unique properties [5]–[8]. By adjusting the magnitude and direction of the external magnetic field, one can efficiently and reversibly control the self-assembly process of the superparamagnetic colloidal particles and adjust the lattice parameters and the symmetry of photonic crystal to obtain the magnetic responsive photonic crystals with ideal optical properties [6], [9]–[11]. Ge *et al.* [12]–[18] reported the superparamagnetic Fe_3O_4 colloidal photonic crystal with the magnetically tunable PBGs covering the visible region. They prepared the superparamagnetic Fe_3O_4 clusters which composed of many primary Fe_3O_4 nanospheres of 10 nm. The clusters can increase the magnetic response and the interaction of particles, and avoid the superparamagnetic-to-ferromagnetic transition (the critical size of Fe_3O_4 with superparamagnetism is 30 nm). Given to the strict experimental conditions and poor repeatability, we used the relatively simple high-temperature pyrolysis method [19]–[23] to synthesize the hollow carbon-coated Fe_3O_4 colloidal particles, expecting to obtain the magnetically responsive colloidal photonic crystal. The composite particles exhibit typical superparamagnetism and the rich carboxyl and hydroxyl groups introduce the strong electrostatic repulsion on the surface. When the magnetic forces and electrostatic repulsion force reach the balance, the carbon-coated superparamagnetic colloidal particles can be self-assembled to form the chain-like photonic crystal. And the external conditions [24]–[27] that can change the balance between nanoparticles will cause the variety of the photonic crystal structure and affect its optical transmission characteristics.

In this paper, based on the composite particles as-prepared in experiments, we numerically simulate the optical transmission characteristic of the hollow carbon-coated Fe_3O_4 colloidal photonic crystal using the FDTD method, and investigate the influence of different structural parameters on PBGs, including the lattice constant, the number of period, the thickness of carbon layer and Fe_3O_4 cluster layer and the thickness ratio of the two layers. The results offer the optimal structure parameters of the photonic crystal and provide theoretical reference for designing the experimental programs to fabricate this kind of colloidal photonic crystal with ideal PBG property.

2. Methods and Models

The FDTD method [28], [29] was first proposed by K. S. Yee in 1966, and it is one of the most classical simulation methods of electromagnetic field [30]. It starts from the discretization of the Maxwell equations and can produce relatively small errors. The basic idea of FDTD is to directly solve the time-dependent Maxwell equations and replace the differential forms using the central difference forms of the electric and magnetic field components in time and space. After the discretization of the electric and magnetic field components in time and space by alternating sampling, each electric field component is surrounded by four magnetic field components and each magnetic field component is surrounded by four electric field components, making the space of electromagnetic field as the Yee grid distribution. Therefore, a set of differential equations are used to express the time-dependent Maxwell equations and then we solve the electromagnetic field in space under the step-by-step drive in the axis of time. According to the initial values and the boundary conditions, we can gradually obtain the distribution of the electromagnetic field in space at each time [31]–[33].

The simulation models originate from the structure of the carbon-coated Fe_3O_4 nanoparticles prepared in our previous experiments. In synthesis, 0.30 g of ferrocene $(Fe(C_5H_5)_2)$ was dissolved in 30 mL of acetone (C_3H_6O). After sonication for 30 min, 1.50 mL of hydrogen peroxide (H_2O_2, 30%) was gradually added into the above mixture solution, and at the same time using the magnetic stirring device to vigorously stirred for 30 min. Then the mixture solution was transferred into the Teflon-lined stainless autoclave with the volume of 50 mL. After that, the autoclave was heated to 200 °C and maintained for 72 h, and it was then naturally cooled to room temperature. The products from the autoclave were separated as the supernatant and the precipitates

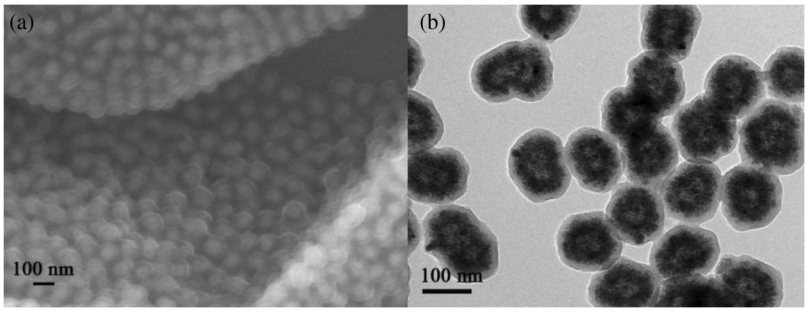

Fig. 1. (a) SEM image and (b) TEM image of the hollow carbon-coated Fe_3O_4.

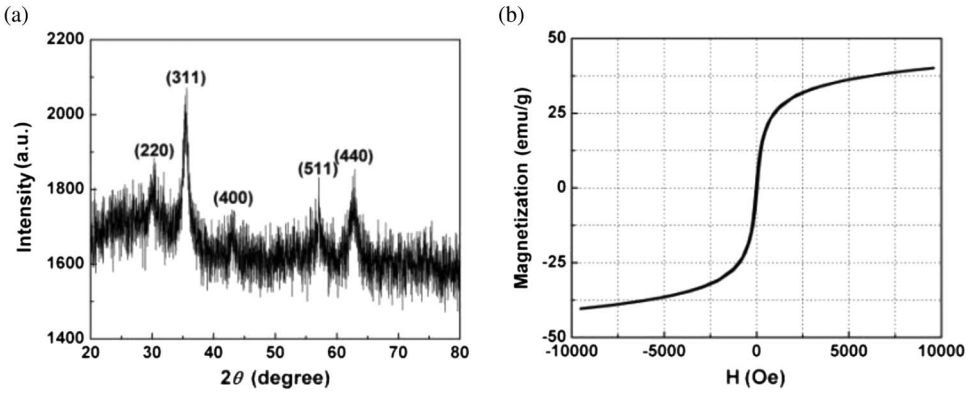

Fig. 2. XRD pattern (a) and magnetic hysteresis (b) of the hollow carbon-coated Fe_3O_4.

under a magnetic field, and then the supernatant was discarded. In order to remove the excess ferrocene, the precipitates were then washed several times with acetone. The final black products were dried at room temperature in a vacuum oven and then are characterized by SEM, TEM, XRD, and VSM. Fig. 1(a) shows the representative SEM image of the Fe_3O_4 nanoparticles which are coated with carbon layer on the surface. Fig. 1(b) shows the typical TEM image of the sample, which demonstrates that the Fe_3O_4 cluster is not the solid structure, but the hollow structure which composed of the carbon layer on its surface, Fe_3O_4 cluster layer and hollow body inside it. Fig. 2(a) shows the XRD patterns of the as-prepared samples and the characteristic peaks indicate that the Fe_3O_4 is formed. The hysteresis loop of the sample in Fig. 2(b) measured at room temperature indicates that the sample displays the superparamagnetism, which means it can perform instant response to external magnetic fields.

In addition, the carbon layer offers the surface modification for the Fe_3O_4 clusters, and it can simultaneously introduce the electrostatic repulsion and steric effects on the surface. The rich carboxyl and hydroxyl groups on the surface provide the high density of negative charge. Thus, the particles prepared in our previous work can reach the balance of the electrostatic repulsion force and the magnetic forces under the external magnetic field to self-assemble into photonic crystal and display the apparent colors just as shown in Fig. S1 in the Supporting Information. The average radius of the hollow body $r = 10$ nm, and it is less affected by the experimental conditions.

The simulation models are created as those depicted in Fig. 3. The composite nanoparticles are periodically arranged into the cubic lattice in air with lattice constant a along x, y, z directions. The number of the period is N and the boundary conditions along x, y, z directions are the electrical boundary, open boundary and magnetic boundary, respectively. The incident

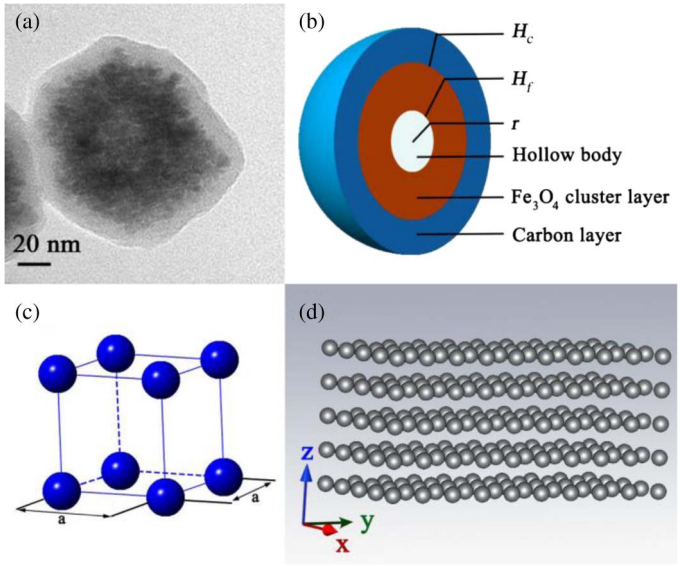

Fig. 3. TEM image (a) and the simulation model (b) of single composite particle. Cell structure (cubic lattice) of photonic crystal arranged by composite particles (c). Photonic crystal array in space (d).

electromagnetic wave propagates along the *y*-direction and its frequency falls in the visible range 395 THz $\sim$ 770 THz.

The Debye relaxation relation [34]–[36] between the complex permittivity of materials and the frequency is as follows:

$$\varepsilon_r^* = \varepsilon_\infty + (\varepsilon_s - \varepsilon_\infty)/(1 + i\omega\tau)$$

$$\varepsilon_r'(\omega) = \varepsilon_\infty + (\varepsilon_s - \varepsilon_\infty)/(1 + \omega^2\tau^2)$$

$$\varepsilon_r''(\omega) = (\varepsilon_s - \varepsilon_\infty)\omega\tau/(1 + \omega^2\tau^2)$$

where ε_∞ and ε_s are the real part of the optical-frequency and static permittivity, respectively. i is the imaginary unit $\sqrt{-1}$. ω and τ are the frequency and relaxation time, respectively. From the Debye relaxation relation, the electric field changes very fast at high-frequency range, and its changing cycle is almost shorter than the relaxation time. As a result, the relaxation polarization cannot keep up with the change of electric field and only the instantaneous polarization can occur. The imaginary part of the permittivity tends to zero for the optical frequency and this means that the loss is so small that it can be neglected. Therefore, in this paper the electromagnetic loss in propagation can be overlooked and the permittivity is set as constant. The relative permittivity of hollow body, Fe_3O_4 clusters layer and carbon layer are 1, 12.25, and 6.4 [37], respectively. The relative permeability of the three materials is 1 in optical frequency range [38]. We use the adaptive mesh refinement calculation, and the error precision is 0.02. The inhomogeneous grid division [39] provide the reasonable utilization of the computer resource, and improve the calculation speed at the premise of ensuring the calculation precision.

3. Results and Discussions

3.1. The Influence of the Lattice Constant

In the process of building models, we make reference to the experimental data and set the parameters as follows: the composite particles are arranged into cubic lattice with the lattice

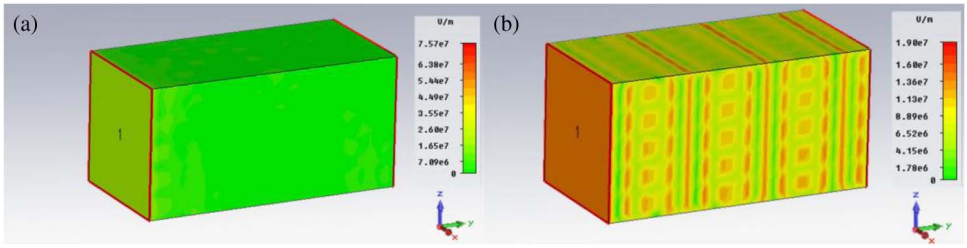

Fig. 4. Visibility graph of the electromagnetic wave with the frequency (a) $f = 680$ THz inside and (b) $f = 580$ THz outside PBGs.

constant $a = 300$ nm, and the number of the period $N = 5 \times 10 \times 5$. The thickness of Fe_3O_4 cluster layer H_f and carbon layer H_c are 40 nm and 25 nm, respectively. After the setting of incentive and the boundary conditions, the adaptive mesh refinement system divides the grid into 1 474 200 mesh cells, and the minimum size of the grid is 10 nm. The time step is 2.17×10^{-17} s, and the maximum number of time steps is 17 493.

The spectrum in Fig. 5(c) shows that the stop band of the photonic crystal appears in 669 THz $\sim$ 702 THz. The electromagnetic wave cannot propagate in the structure as its frequency falling into the PBGs, while it can propagate well as the frequency outside the PBGs. When the electromagnetic wave with the frequency of $f = 680$ THz that is inside the PBGs enters into the photonic crystal, we can only obtain the electromagnetic signal at the incident port, but it decays quickly to zero and the transmission of this electromagnetic wave is inhibited, just as shown in Fig. 4(a). While the electromagnetic wave with the frequency of $f = 580$ THz that is outside the PBGs can propagate well in the structure and we can detect the obvious electromagnetic signals across the whole photonic crystal, just as shown in Fig. 4(b). The animate field of $f = 680$ THz and $f = 580$ THz are shown as a video in the Supporting Information (j.avi and t.avi).

Furthermore, we set the lattice constant as the sweeping parameter that changes from 200 nm $\sim$ 450 nm, and the increment is 50 nm. According to the adaptive mesh refinement calculation, the stop bands appear in 720 THz $\sim$ 770 THz for $a = 200$ nm, 688 THz $\sim$ 763 THz for $a = 250$ nm, 669 THz $\sim$ 702 THz and 751 THz $\sim$ 770 THz for $a = 300$ nm, 654 THz $\sim$ 673 THz and 699 THz $\sim$ 760 THz for $a = 350$ nm, and 660 THz $\sim$ 702 THz for $a = 400$ nm, just as those depicted in Fig. 5.

The optical transmission spectra perform the tendency of moving to the low-frequency direction and the position of PBGs gradually red shifts with the increasing a. The bandwidth first increases and then decreases. The photonic crystal can perform good PBG property for a varying between 200 nm and 400 nm. However, with the further increase of lattice constant, the PBGs gradually become disorganized (see Fig. S2 in the Supporting Information). When a reaches to 450 nm, the spectrum loses regularity and PBGs seems to be disorganized. This can be explained by the Bragg diffraction mechanism which is the essential reason for the formation of the photonic band gap. The Bragg diffraction is mutually influenced by the amplitude of the reflected and refracted light and the lattice constant. With the increase of lattice constant, the phase relationship of the reflected and refracted lights gradually became mismatched. Therefore, the interference phenomenon cannot occur and thus the Bragg diffraction cannot be observed. Therefore, the PBGs lost organized state for larger lattice constant.

We can also qualitatively analyze the dependence of the diffraction wavelength on the lattice constant from the Bragg's law [12] $\lambda = 2nd \sin\theta$, in which λ, n, d, θ are the diffraction wavelength, the refractive index of the medium, the lattice plane spacing and the Bragg angle, respectively. Thus, the diffraction wavelength increases with the increasing lattice plane spacing, showing the tendency of red-shift for the transmission spectra. The calculation results are

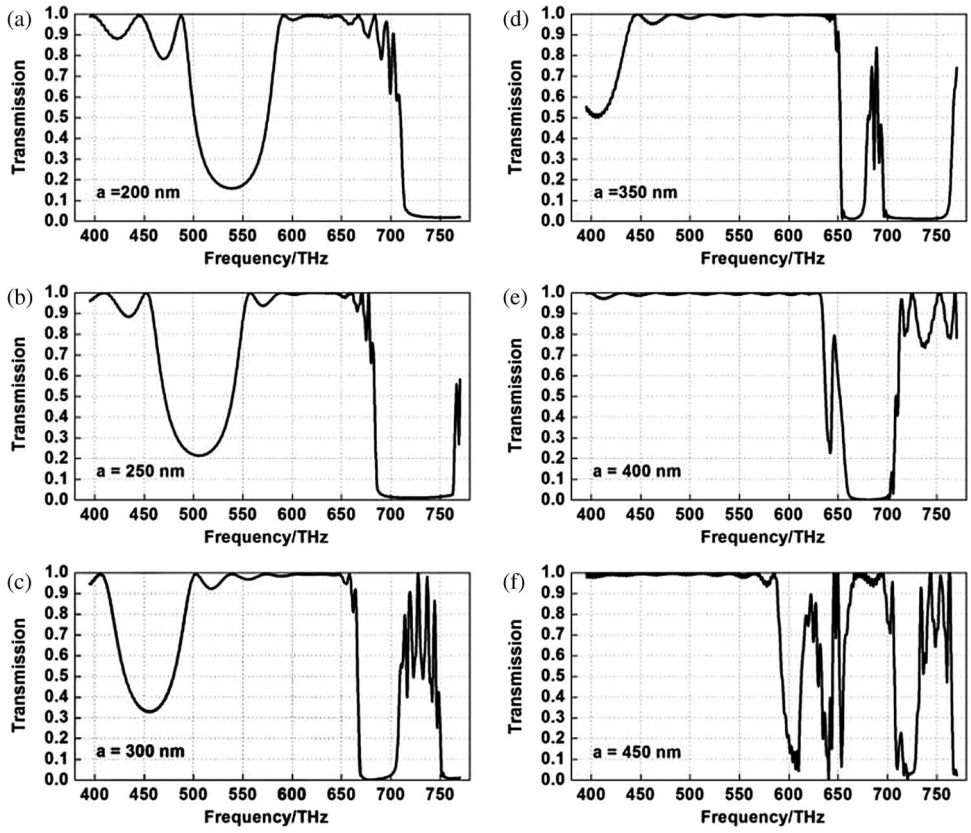

Fig. 5. (a)–(f) Optical transmission spectra of photonic crystal with different lattice constant a of 200, 250, 300, 350, 400, and 450 nm.

consistent with the theoretical results and the experimental results [12], and they are reliable to guide the design of the experimental schemes.

3.2. The Influence of the Number of the Period

Considering that the electromagnetic wave propagates along y-direction in photonic crystal, we set the number of the building block along y-direction as the sweeping parameter to obtain its influence laws on the optical transmission characteristics. The composite particles, in which the radius of the hollow body is 10 nm, the thickness of Fe_3O_4 cluster layer is 40 nm and carbon layer is 25 nm, periodically arranged into the cubic lattice structure with $a = 300$ nm. The number of the period in x-direction $N_x = 5$ and z-direction $N_z = 5$, while in y-direction N_y varies from 2 to 20 to get the influence of the period in propagating direction on the PBGs.

The calculated results show that the photonic crystal performs one irregular band gap when N_y is less than 5 and it gradually develops into regular state with the increasing N_y, just as Fig. 6(a). When N_y is larger than 5 and ranging from 5 to 20 in Fig. 6(b), the regular band gap appears in 670 THz $\sim$ 705 THz, which means that the position of the band gap and its bandwidth have remained basically unchanged with the increase of N_y. Both the number of the oscillations on two sides of the band gap and the depth of the band gap in the low-frequency range show obvious increase with the increasing N_y. Given to the two factors that obtaining the regular band gap and saving the computer memory to improve the calculating speed, we set $N_y = 10$ to simulate in other parts of this paper.

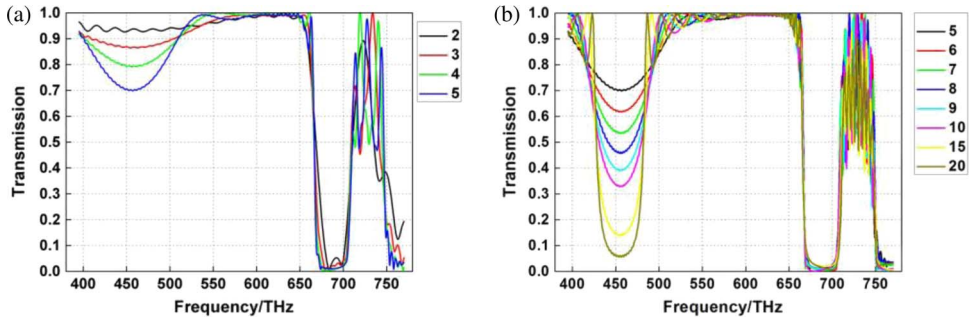

Fig. 6. Optical transmission spectra of photonic crystal with different N_y of (a) 2 $\sim$ 5 and (b) 5 $\sim$ 20.

3.3. The Influence of the Structure Parameters of the Composite Particle

3.3.1. The Carbon Layer Thickness

Experimental results show that adjusting the amount of a certain reactant can correspondingly change the carbon layer thickness during the preparation of hollow carbon-coated Fe_3O_4 spheres. The variety of the carbon layer thickness will undoubtedly change the effective permittivity of the composite particle, and finally results in relevant impacts on the PBGs. In this part, we study the influence of the carbon layer thickness on the optical transmission characteristic of this kind of colloidal photonic crystal by FDTD. The parameters of the model are set as follows: $a = 300$ nm and the radius of the hollow body is $r = 10$ nm. The thickness of Fe_3O_4 clusters layer H_f is 40 nm, while the thickness of the carbon layer H_c is the sweeping parameter. Given to the fact that the carbon layer thickness is about 10 nm $\sim$ 35 nm in experiments, H_c varies from 5 nm to 40 nm in simulation. The periodic number of the structure is $N = 5 \times 10 \times 5$. The grid is divided into 5 009 724 grid cells and the minimum grid size is 5.0 nm.

Fig. 7 shows the optical transmission spectra of photonic crystal with different carbon layer thickness (5 nm $\sim$ 40 nm). The spectra show that the stop bands gradually move towards the low-frequency direction and the corresponding bandwidth becomes larger with the increase of the carbon layer thickness. There is no obvious stop band in the transmission spectrum as $H_c = 5$ nm and the minimum transmittance is 0.32. Therefore, the photonic crystal cannot perform the obvious diffraction phenomenon for smaller thickness of the carbon layer. While the clear stop band appears and the diffracted light can be available as $H_c = 10$ nm $\sim$ 25 nm. And the position of the same stop band moves from 760 THz $\sim$ 767 THz to 669 THz $\sim$ 702 THz, while the corresponding bandwidth increases from 7 THz to 33 THz. When H_c is greater than 25 nm, there are two stop bands in the visible range and both of them show the trend of red-shift and increasing bandwidth. The variety of the carbon layer thickness can perform obvious impact to the stop band of the photonic crystal. Therefore, when other parameters are fixed, we can effectively adjust the diffraction wavelength in the visible range by changing the thickness of the carbon-coated layer.

From the above results, we can get the significant conclusions to guide further experiments. For the colloidal photonic crystal with hollow carbon-coated Fe_3O_4 as building blocks, the thickness of carbon layer plays an important role in adjusting the optical transmission property. The range of diffraction wavelength prefers to appear in blue-violet light for the smaller carbon layer thickness. Conversely, it tends to appear in red-yellow light for the larger one. Furthermore, 10 nm $\sim$ 25 nm is the optimal thickness of the carbon layer, and in this situation the colloidal photonic crystal exhibits uniform color response with the obvious single stop band in the transmission spectrum. Thus, we can try to adjust the carbon layer thickness by controlling the react conditions to achieve the ideal photonic crystal.

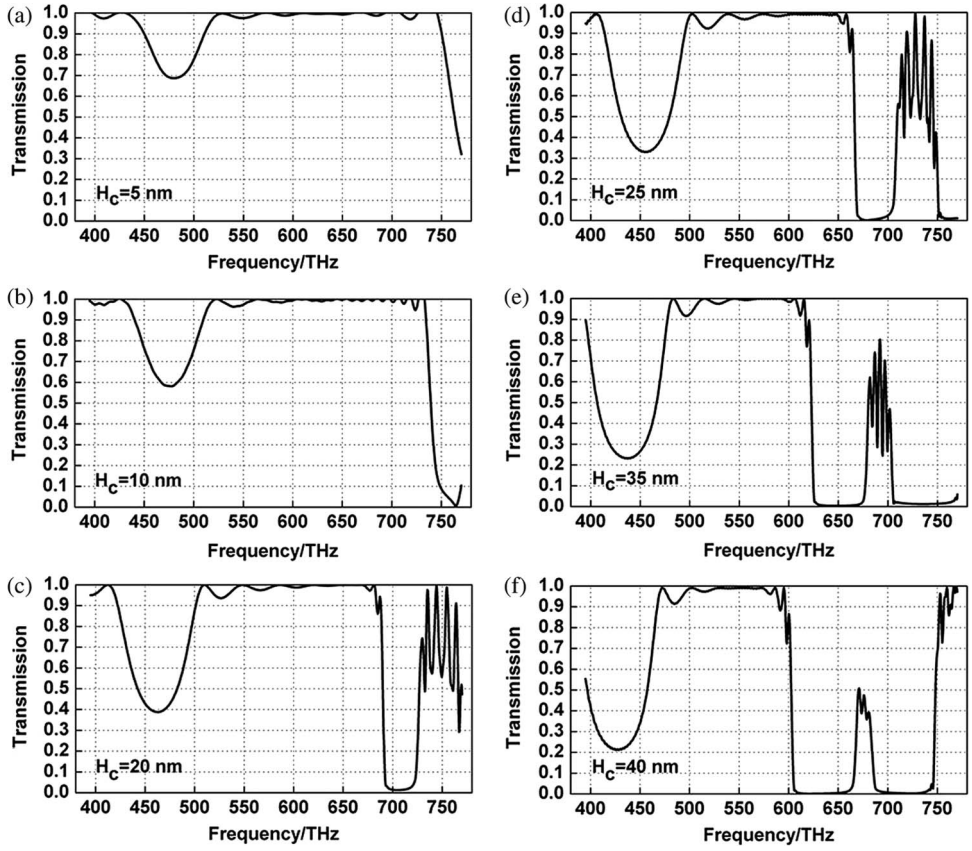

Fig. 7. (a)–(f) Transmission spectra of photonic crystal with different carbon layer thickness H_c of 5, 10, 20, 25, 35, and 40 nm.

3.3.2. *The* Fe_3O_4 *Cluster Layer Thickness*

The other important structural parameter that can be adjusted in experiments is the thickness of Fe_3O_4 cluster layer in the hollow structure. The larger the thickness of Fe_3O_4 cluster is, the more it contains the primary Fe_3O_4 nanocrystals. The particles will response to the magnetic field more sensitive and it is more possible to obtain the photonic crystal with high performance. In this part, we study the influence of Fe_3O_4 cluster layer thickness on the optical transmission property by FDTD.

In the process of building model, the relative permittivity and permeability of the materials are just as before. The model is the cubic lattice with $a = 300$ nm and the periodic number of the structure is $N = 5 \times 10 \times 5$. The thickness of carbon layer $H_c = 25$ nm. The thickness of Fe_3O_4 cluster layer H_f is the sweeping parameter varying from 15 nm to 65 nm with the increment is 10 nm in the simulation.

According to the adaptive mesh refinement calculation with the error precision of 0.02, the transmission spectra of the photonic crystal with different Fe_3O_4 cluster layer thickness H_f are presented in Fig. 8. The changing trend of the stop bands is towards the low-frequency direction and the stop bands continuously move from the near-ultraviolet region to the visible region, then from the visible region to near-infrared region with the increasing H_f. At the same time, the first bandwidth gradually increases while the second decreases. It can be seen from the spectra distribution that there are no obvious stop bands as $H_f \leq 25$ nm and the minimum transmittance is 0.58. Then the obvious single stop band appears in 723 THz $\sim$ 744 THz as $H_f = 35$ nm. Two or more stop bands emerge in the visible range for $H_f \geq 45$ nm, and when H_f reaches to 65 nm, the spectrum is divided by four stop bands, resulting in the fact that uniform stop bands cannot appear and that the transmission spectra become less regular.

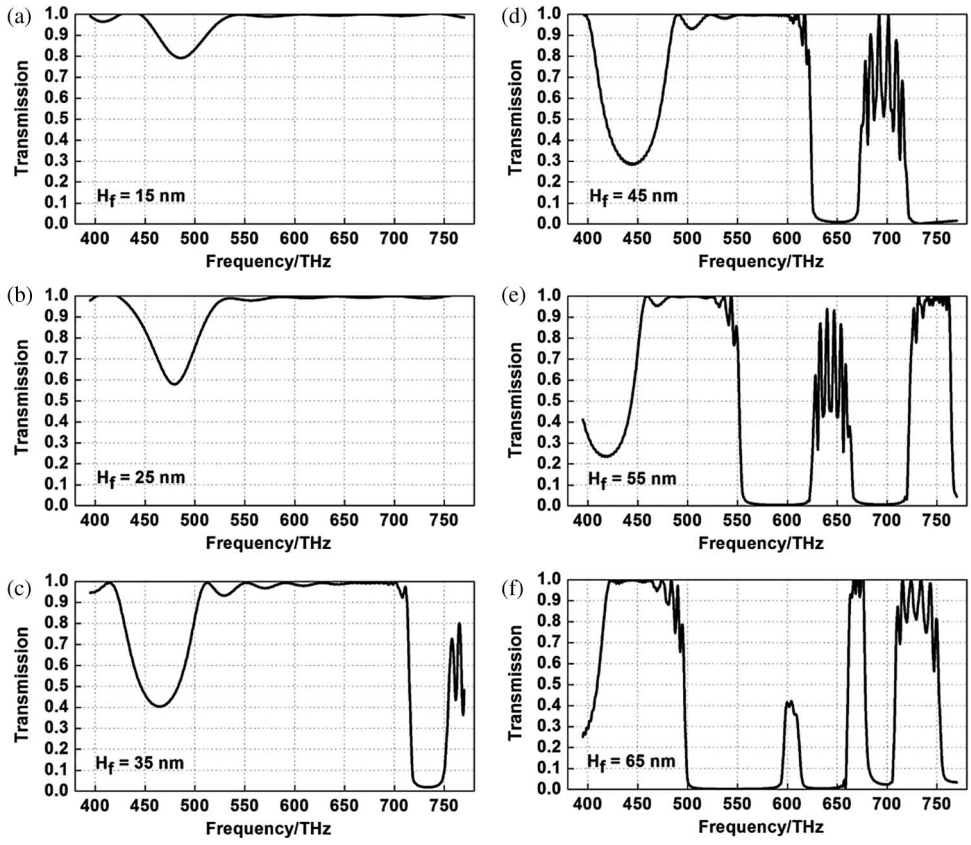

Fig. 8. (a)–(f) Transmission spectra of photonic crystal with different Fe_3O_4 cluster layer thickness H_f of 15, 25, 35, 45, 55, and 65 nm.

Actually the increasing thickness of Fe_3O_4 cluster layer which has larger permittivity than other constituent materials can result in the larger effective permittivity of the composite particles. This will directly increase the permittivity contrast between the particles and the background, which is benefit to the appearance of PBGs. Moreover, the total size of the composite particle enlarges for the increasing Fe_3O_4 cluster layer thickness, and thus, the chances for Bragg diffraction increase accordingly. In this situation, more lights can be reflected and refracted, resulting in the appearance of multiple PBGs. Therefore, it is not benefit to the appearance of uniform stop bands for too small or large thickness of Fe_3O_4 clusters layer. The optimal thickness is 35 nm $\sim$ 55 nm when other parameters are fixed, and the diffracted wavelength tends to appear in short wavelength range for the smaller thickness, while it appears in long wavelength range for the larger one.

3.3.3. The Thickness Ratio

Given to the actual experimental results and the above simulated results, we study the influence of the thickness ratio of the carbon layer and Fe_3O_4 cluster layer on the transmission property of the photonic crystal. And based on the simulation results, we expect to get the optimal thickness ratio to find a fine balance between the two layers. The radii of the hollow body and the whole composite particle are $r = 10$ nm and $R = 75$ nm, respectively. Thus the thickness sum of the two layers keeps as a constant, namely $H_c + H_f = 65$ nm. The lattice constant a is 300 nm and the period $N = 5 \times 10 \times 5$. According to the numerical simulation with FDTD, the calculated results are showed in Fig. 9.

For the photonic crystal structure composed of the composite particles without the carbon layer on the surface, the thickness ratio $H_c : H_f = 0$ nm : 65 nm and there are two stop bands of 567

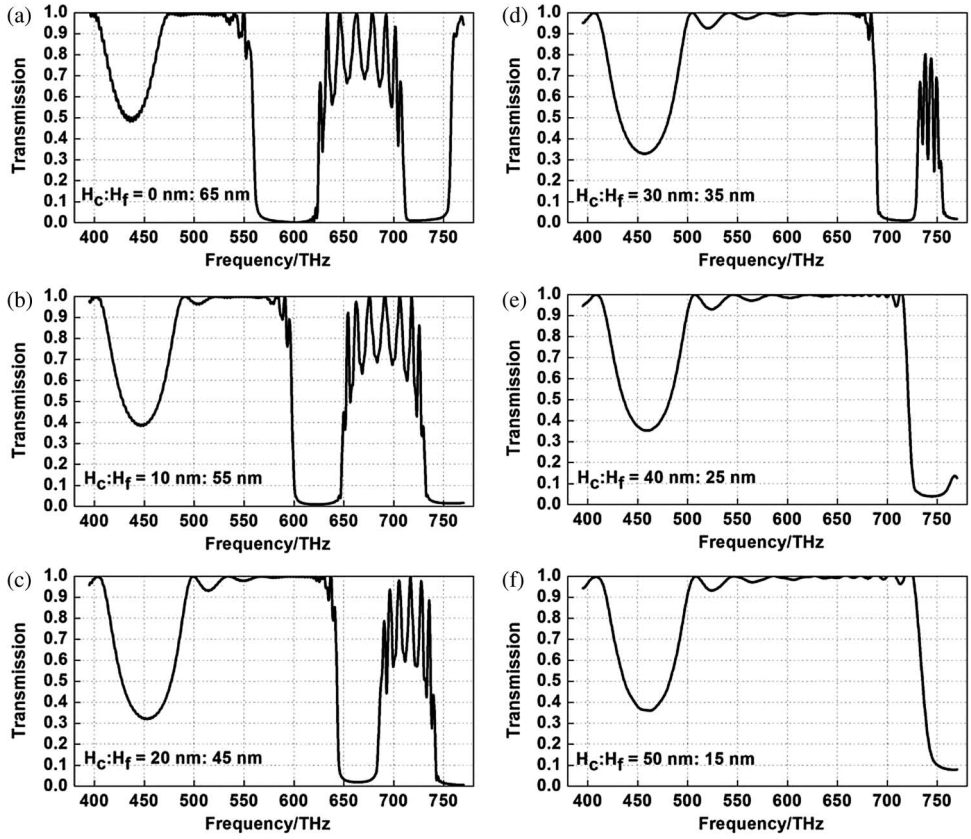

Fig. 9. (a)–(f) Transmission spectra of photonic crystal with different thickness ratio $H_c : H_f$ of 0 : 65, 10 : 55, 20 : 45, 30 : 35, 40 : 25, and 50 : 15.

THz $\sim$ 621 THz and 712 THz $\sim$ 750 THz appeared in the visible range. The transmission spectra gradually move to the high-frequency direction with the increase of the thickness ratio $H_c : H_f$. And the bandwidth of the two stop bands decreases until they move outside the visible range. The first stop band appears in 603 THz $\sim$ 644 THz for $H_c : H_f = 10$ nm : 55 nm, 651 THz $\sim$ 677 THz for $H_c : H_f = 20$ nm : 45 nm and 694 THz $\sim$ 727 THz for $H_c : H_f = 30$ nm : 35 nm. However, for $H_c : H_f = 40$ nm : 25 nm and $H_c : H_f = 50$ nm : 15 nm, there are no complete stop bands in the visible region. To get the ideal PBG property, the optimal thickness ratio is $H_c : H_f = 10$ nm : 55 nm in which the system possesses complete PBGs and wider bandwidth.

The results can be explained with the effective permittivity. The relations of the refractive index n with permittivity ε of the material and the effective permittivity [40] of composite particles are as follows:

$$n = \sqrt{\varepsilon\mu}$$

$$n_{\text{effective}} = \frac{r_{\text{core}}^3}{r_{\text{core-shell}}^3} n_{\text{core}} + \left(1 - \frac{r_{\text{core}}^3}{r_{\text{core-shell}}^3}\right) n_{\text{shell}}$$

where μ is the permeability of the material. r and n are the radius and refractive index of materials in each part of the composite particles, respectively. With the increase of the thickness ratio $H_c : H_f$, the effective permittivity of the particles decreases and PBGs show the blue-shift trend, which is in line with our earlier work. The Fe_3O_4 cluster layer plays more important role in the appearance of PBGs, but considering from the perspective of experiments, the carbon layer is necessary for offering the rich negative charges to generate the electrostatic repulsion force.

4. Conclusion

The optical transmission characteristics for photonic crystal with hollow carbon-coated Fe_3O_4 colloidal spheres as building block have been calculated with FDTD method. The transmission properties with different parameters have been analyzed, including the lattice constant, the number of the period in propagating direction, the structural parameters of particles (the surface carbon layer thickness, the Fe_3O_4 clusters layer thickness and the thickness ratio of the two layers). The results show that this kind of colloidal photonic crystal performs good PBG characteristic and the stop bands show red-shift with the increase of the lattice constant while the bandwidth first increases and then decreases. With the increasing number of the period in propagating direction, the photonic crystal generates the PBG changing from irregular to uniform, the number of the oscillations on both sides of PBG increases and the PBG in the low-frequency region is deepened. To obtain the regular PBG and save the computer memory to improve the calculating speed, the optimal N_y is set as 10 for the simulation in the paper. Photonic crystals with small thickness of carbon layer preferentially diffract blue-violet light, while the large one preferentially diffracts red-yellow light. The PBGs show red-shift and the optimal thickness of carbon layer that can make the uniform color appear is 10 nm $\sim$ 25 nm. The PBGs also red shift with the increasing thickness of Fe_3O_4 cluster layer, and the first bandwidth increases while the second decreases. The PBGs develop from the initial single uniform stop band to simultaneously appearing two or more stop bands in the visible region. The optimal thickness of Fe_3O_4 clusters layer for the ideal uniform PBG is 35 nm $\sim$ 55 nm. The best thickness ratio of the two layers is $H_c : H_f = 10$ nm : 55 nm for the complete PBG and wider bandwidth. The calculated results provide the significant theoretical guidance for designing experiments to prepare the photonic crystals with the desirable PBG properties.

References

[1] E. Yablonovitch, "Inhibited spontaneous emission in solid-state physics and electronics," *Phys. Rev. Lett.*, vol. 58, no. 20, pp. 2059–2062, May 1987.

[2] S. John, "Strong localization of photons in certain disordered dielectric superlattices," *Phys. Rev. Lett.*, vol. 58, no. 23, pp. 2486–2489, Jun. 1987.

[3] K. M. Ho, C. T. Chan, and C. M. Soukoulis, "Existence of a photonic gap in periodic dielectric structures," *Phys. Rev. Lett.*, vol. 65, no. 25, pp. 3152–3155, Dec. 1990.

[4] E. Yablonovitch, T. J. Gmitter, and K. M. Leung, "Photonic band structure: The face-centered-cubic case employing nonspherical atoms," *Phys. Rev. Lett.*, vol. 67, no. 17, pp. 2295–2298, Oct. 1991.

[5] L. He *et al.*, "Assembly and photonic properties of superparamagnetic colloids in complex magnetic fields," *Langmuir*, vol. 27, no. 22, pp. 13 444–13 450, Oct. 2011.

[6] L. He, M. S. Wang, J. P. Ge, and Y. D. Yin, "Magnetic assembly route to colloidal responsive photonic nanostructures," *Accounts Chemical Res.*, vol. 45, no. 9, pp. 1431–1440, Nov. 2012.

[7] T. X. Liu, X. L. Gong, Y. G. Xu, and S. H. Xuan, "Magneto-induced stress enhancing effect in a colloidal suspension of paramagnetic and superparamagnetic particles dispersed in a ferrofluid medium," *Soft. Matter.*, vol. 10, pp. 813–818, Nov. 2013.

[8] L. Ye *et al.*, "Real time monitoring of superparamagnetic nanoparticle self-assembly on surfaces of magnetic recording media," *J. Appl. Phys.*, vol. 115, no. 17, Feb. 2014, Art. ID. 17B513.

[9] M. S. Wang, L. He, and Y. D. Yin, "Magnetic field guided colloidal assembly," *Mater. Today*, vol. 16, no. 4, pp. 110–116, Apr. 2013.

[10] W. Luo *et al.*, "Steric-repulsion-based magnetically responsive photonic crystals," *Adv. Mater.*, vol. 26, no. 7, pp. 1058–1064, Feb. 2014.

[11] H. B. Hu, H. Zhong, C. L. Chen, and Q. W. Chen, "Magnetically responsive photonic watermarks on banknotes," *J. Mater. Chemistry C.*, vol. 2, pp. 3695–3702, Jan. 2014.

[12] J. P. Ge and Y. D. Yin, "Responsive photonic crystals," *Angewandte Chemie Int. Ed.*, vol. 50, no. 7, pp. 1492–1522, Feb. 2011.

[13] J. P. Ge, L. He, J. Goebl, and Y. D. Yin, "Assembly of magnetically tunable photonic crystals in nonpolar solvents," *J. Amer. Chemical Soc.*, vol. 131, no. 10, pp. 3484–3486, Feb. 2009.

[14] J. P. Ge, Y. X. Hu, T. R. Zhang, T. Huynh, and Y. D. Yin, "Self-assembly and field-responsive optical diffractions of superparamagnetic colloids," *Langmuir*, vol. 24, no. 7, pp. 3671–3680, Feb. 2008.

[15] J. P. Ge *et al.*, "One-step synthesis of highly water-soluble magnetite colloidal nanocrystals," *Chemistry A Eur. J.*, vol. 13, no. 25, pp. 7153–7161, Jun. 2007.

[16] J. P. Ge, Y. X. Hu, M. Biasini, W. P. Beyermann, and Y. D. Yin, "Superparamagnetic magnetite colloidal nanocrystal clusters," *Angewandte. Chemie Int. Ed.*, vol. 46, no. 23, pp. 4342–4345, Apr. 2007.

[17] H. Wang, Q. W. Chen, Y. F. Yu, K. Cheng, and Y. B. Sun, "Size- and solvent-dependent magnetically responsive optical diffraction of carbon-encapsulated superparamagnetic colloidal photonic crystals," *J. Phys. Chemistry C.*, vol. 115, no. 23, pp. 11 427–11 434, May 2011.
[18] H. B. Hu *et al.*, "Invisible photonic printing: Computer designing graphics, UV printing and shown by a magnetic field," *Sci. Rep.*, vol. 3, no. 1484, pp. 1–5, Mar. 2013.
[19] K. Cheng *et al.*, "Preparation and biological characterization of hollow magnetic Fe_3O_4@C nanoparticles as drug carriers with high drug loading capability, pH-control drug release and MRI properties," *Biomater. Sci.*, vol. 1, no. 9, pp. 965–974, Jun. 2013.
[20] H. B. Hu, C. L. Chen, and Q. W. Chen, "Magnetically controllable colloidal photonic crystals: Unique features and intriguing applications," *J. Mater. Chemistry C.*, vol. 1, pp. 6013–6030, May 2013.
[21] R. Li *et al.*, "Pd-Fe_3O_4@C hybrid nanoparticles: Preparation, characterization, and their high catalytic activity toward Suzuki coupling reactions," *J. Mater. Chemistry*, vol. 22, pp. 22 750–22 755, Sep. 2012.
[22] J. Liu, Y. W. Mao, and J. P. Ge, "Electric field tuning of magnetically assembled photonic crystal," *J. Mater. Chemistry C*, vol. 1, pp. 6129–6135, Apr. 2013.
[23] C. Ma *et al.*, "Centrifugation-induced water-tunable photonic colloidal crystals with narrow diffraction bandwidth and highly sensitive detection of SCN^-," *ACS Appl. Mater. Interfaces*, vol. 5, no. 6, pp. 1990–1996, Feb. 2013.
[24] D. M. Sullivan, *Electromagnetic Simulation Using the FDTD Method*. Hoboken, NJ, USA: Wiley, 2000.
[25] K. S. Yee, "Numerical solution of initial boundary value problems involving Maxwell's equations in isotropic media," *IEEE Trans. Antennas Propag.*, vol. 14, no. 3, pp. 302–307, May 1966.
[26] C. Geng *et al.*, "Large-area and ordered sexfoil pore arrays by spherical-lens photolithography," *ACS Photon.*, vol. 1, no. 8, pp. 754–760, Aug. 2014.
[27] L. C. Yang, C. C. Huang, H. C. Huang, and S. L. Tsao, "FDTD simulation of time varying optical vortex phenomena in SOI photonic crystal structures," *Optik—Int. J. Light Electron Opt.*, vol. 122, pp. 924–927, Jun. 2011.
[28] K. Gehlot and A. Sharma, "Analysis of 2D photonic bandgap waveguides using a simple analytical method," in *Proc. Int. Conf. Fiber Opt. Photon.*, 2012, pp. 1–3.
[29] M. B. Yan, Z. T. Fu, and C. L. Xu, "Study on maximum band gap of two-dimensional photonic crystal with elliptical holes," *Optik—Int. J. Light and Electron Opt.*, vol. 124, no. 23, pp. 5972–5975, Dec. 2013.
[30] Y. Lin, H. B. Yang, J. F. Zhu, and F. Wang, "$Y_3Fe_5O_{12}$/$BaFe_{12}O_{19}$ composite with giant dielectric constant and high magnetization," *Mater. Lett.*, vol. 93, pp. 230–232, Feb. 2013.
[31] T. Bauer, M. Michl, P. Lunkenheimer, and A. Loidl, "Nonlinear dielectric response of Debye, α, and β relaxation in 1-propanol," *Proc. J. Non-Cryst. Solids*, Jul. 2014, pp. 1–8.
[32] J. Y. Fu, "On the theory of the universal dielectric relaxation," *Philos. Mag.*, vol. 94, no. 16, pp. 1788–1815, Apr. 2014.
[33] C. S. Kee, J. E. Kim, H. Y. Park, I. Park, and H. Lim, "Two-dimensional tunable magnetic photonic crystals," *Phys. Rev. B.*, vol. 61, no. 23, pp. 15 523–15 525, Jun. 2000.
[34] R. Z. Yue, M. Feng, and H. B. Zhan, "Numerical and simulation study on silver nanoparticles composite metamaterial," *Photon. Sinica*, vol. 40, no. 12, pp. 1860–1864, Dec. 2012.
[35] W. D. Wang, J. X. Wang, Y. Li, and H. Mao, "Convolutional perfectly matched layer absorbing boundary condition of the finite-difference time-domain method for the microstrip antenna," in *Proc. Int. Conf. IEEE CMCSN*, 2012, pp. 125–128.
[36] M. G. Han *et al.*, "Full color tunable photonic crystal from crystalline colloidal arrays with an engineered photonic stop-band," *Adv. Mater.*, vol. 24, no. 48, pp. 6438–6444, Oct. 2012.